

ORIGINAL ARTICLE

Plasma SARS-CoV-2 RNA elimination and RAGE kinetics distinguish COVID-19 severity

Xiaoyan Deng^{1,2,a} , Pierre Gantner^{3,4,a}, Julia Forestell¹, Amélie Pagliuzza^{3,4},
Elsa Brunet-Ratnasingham^{3,4}, Madeleine Durand³, Daniel E Kaufmann^{3,5,6,7}, Nicolas Chomont^{3,4} &
Morgan Craig^{1,2} 

¹Research Centre of the Centre Hospitalier Universitaire Sainte-Justine, Montréal, QC, Canada

²Département de mathématiques et de statistique, Université de Montréal, Montréal, QC, Canada

³Research Centre of the Centre Hospitalier de l'Université de Montréal (CRCHUM), Montréal, QC, Canada

⁴Département de Microbiologie, Infectiologie et Immunologie, Université de Montréal, Montréal, QC, Canada

⁵Centre hospitalier de l'Université de Montréal (CHUM), Montréal, QC, Canada

⁶Département de Médecine, Université de Montréal, Montréal, QC, Canada

⁷Division of Infectious Diseases, Department of Medicine, University Hospital and University of Lausanne, Lausanne, Switzerland

Correspondence

M Craig, Research Centre of the Centre Hospitalier Universitaire Sainte-Justine, Montréal, QC, Canada.
E-mail: morgan.craig@umontreal.ca

^aEqual contributors.

Received 17 March 2023;
Revised 1 September 2023;
Accepted 8 September 2023

doi: 10.1002/cti.1468

Clinical & Translational Immunology
2023; 12: e1468

Abstract

Objectives. Identifying biomarkers causing differential SARS-CoV-2 infection kinetics associated with severe COVID-19 is fundamental for effective diagnostics and therapeutic planning. **Methods.** In this work, we applied mathematical modelling to investigate the relationships between patient characteristics, plasma SARS-CoV-2 RNA dynamics and COVID-19 severity. Using a straightforward mathematical model of within-host viral kinetics, we estimated key model parameters from serial plasma viral RNA (vRNA) samples from 256 hospitalised COVID-19⁺ patients. **Results.** Our model predicted that clearance rates distinguish key differences in plasma vRNA kinetics and severe COVID-19. Moreover, our analyses revealed a strong correlation between plasma vRNA kinetics and plasma receptor for advanced glycation end products (RAGE) concentrations (a plasma biomarker of lung damage), collected in parallel to plasma vRNA from patients in our cohort, suggesting that RAGE can substitute for viral plasma shedding dynamics to prospectively classify seriously ill patients. **Conclusion.** Overall, our study identifies factors of COVID-19 severity, supports interventions to accelerate viral clearance and underlines the importance of mathematical modelling to better understand COVID-19.

Keywords: COVID-19, plasma SARS-CoV-2 RNA, RAGE, SARS-CoV-2 kinetics, viral dynamics model

INTRODUCTION

Throughout the COVID-19 pandemic, the factors leading to severe disease have been the subject of intense study.^{1–4} Particular attention has been

paid to clinical and immunological characteristics of severity, as dysregulated and dysfunctional immune responses are characteristic of poor outcomes.^{5,6} Viral loads measured by nasopharyngeal swabs,^{7,8} bronchioalveolar

lavage,⁹ saliva,¹⁰ and at autopsy¹¹ have also been investigated for their association with SARS-CoV-2 infectivity and COVID-19 severity. In that vein, we have previously established that high plasma viral RNA (vRNA) loads in acute infection courses are tightly associated with fatal outcomes in hospitalised patients with COVID-19.¹² Additionally, Fajnzylber et al.⁴ have shown that plasma viral load is associated with increased COVID-19 severity and mortality. As measuring SARS-CoV-2 viral load in the lower respiratory tract requires invasive procedure (e.g. biopsies or bronchoalveolar lavage), its applicability and translatability are greatly limited when compared to plasma viral load that can be easily obtained from a blood draw. However, the dynamics of vRNA in the plasma and their relationships with key immunological markers and COVID-19 outcomes remain poorly characterised.

In addition to experimental and clinical studies, mathematical and computational modelling have contributed to furthering our understanding of SARS-CoV-2 viral dynamics, COVID-19 severity and treatment/vaccine regimens.^{13–15} A classical approach of viral dynamics, the target-cell limited model, has previously been used to establish the kinetics of other respiratory viruses including influenza,^{16–20} SARS-CoV²⁰ and RSV,²¹ in addition to other virus types. In recent studies, this model and its extensions have quantified key rates of SARS-CoV-2 kinetics,^{13,22–25} including the rate of viral shedding. The association with viral kinetics in the plasma, which are potentially distinct from those in the lungs, and COVID-19 outcomes remains to be delineated. In this study, we address this limitation by applying mathematical modelling to establish potential relationships between plasma SARS-CoV-2 RNA kinetics and COVID-19 outcomes for hospitalised patients.

We have recently reported that high levels of vRNA and markers of tissue injury²⁶ (e.g. the receptor for advanced glycation end products (RAGE)),²⁷ a marker of lung damage, and angiotensin-2 (Ang-2),²⁸ a marker of endothelial dysregulation and sepsis, at specific days postsymptom onset are leading indicators of severe disease burden and mortality.¹² To understand the connection between patient characteristics, COVID-19 severity and plasma vRNA dynamics, we collected serial plasma samples from hospitalised patients and quantified SARS-CoV-2 RNA, RAGE and Ang-2 levels.¹² Using a simple and well-established mathematical model of viral

dynamics,^{16,29} we estimated model parameters using a quantitative framework to investigate the relationship between plasma viral dynamics, particularly plasma SARS-CoV-2 viral clearance rates, markers of severity and outcomes in patients hospitalised with COVID-19. Our results showed key differences in plasma vRNA kinetics among patient cohort subgroups. These include an increase in peak viral loads with increases in disease severity and mortality and, crucially, a marked decrease in the rate of viral clearance associated with COVID-19 severity in hospitalised patients. Furthermore, plasma SARS-CoV-2 RNA kinetics were found to be highly correlated with plasma RAGE concentrations, suggesting that RAGE, an important mediator of pulmonary inflammatory responses,³⁰ is a surrogate marker for both viral dynamics in the plasma and COVID-19 shedding that are predictive of severe COVID-19. This analysis highlights that serial vRNA samples can be used to distinguish COVID-19 severity. Together, our results emphasise the importance of quantitative modelling for understanding and predicting markers of COVID-19 severity with high significance to clinical translation.

RESULTS

Estimated SARS-CoV-2 RNA viral loads AUC predicts severity and death

Viraemia AUC (both N and E transcripts) were inferred in a multiple logistic regression to test prediction of both severity and death. A critical form of COVID-19 was independently predicted by AUC viraemia along with age, sex and Ang-2 AUC (Figure 1a). For both transcripts, we found an approximately fivefold increase in the risk of critical disease for every \log_{10} viraemia AUC unit, and a 10-fold increase for \log_{10} unit increment of Ang-2. Above a threshold of 10 and 9 \log_{10} copies/mL of plasma AUC viraemia (for N and E, respectively), higher rates of critical COVID-19 were observed (Figure 1b). The risk of death because of COVID-19 was also increased by AUC viraemia along with age and Ang-2 AUC (Figure 1c). Above a threshold of 16 and 14 \log_{10} copies/mL of plasma AUC viraemia (for N and E, respectively), a higher risk of death was observed (Figure 1d). Overall, estimating AUC viraemia was proven efficient to predict COVID-19 outcome, with a fourfold increased risk in severity and a fivefold increased risk of death when AUC

viraemia was above the defined thresholds (Figure 1e), whatever the target sequence analysed as both measures strongly correlated together ($r = 0.67$, $P < 0.0001$).

Mathematical modelling successfully predicts plasma SARS-CoV-2 RNA viral loads

Given the relationships established above, we next sought to quantify, validate and predict the dynamics of SARS-CoV-2 RNA in the plasma using a simple mathematical model (Equation 1). To assess the ability of our model to predict plasma vRNA kinetics of hospitalised COVID-19 patients, we first fit V_0 , T_0 , p and d_V to average plasma vRNA concentrations in the full cohort using non-linear least squares (Methods and Figure 2b). Across model predictions in the full cohort and in each of the subgroups, p and T_0 were found to remain consistent, suggesting that differences in viral kinetics across groups could be explained entirely by differences in viral inoculation and clearance rates. We then fixed T_0 and p in the remaining analyses (parameter values see Table 1) and estimated the population parameters (i.e. the initial viral load (V_0) and clearance rate (d_V)) for each subgroup using a non-linear mixed-effects model in Monolix (see Methods). Afterwards, the 95% confidence intervals of (V_0) and (d_V) for each population were derived from an estimation of the Fisher Information Matrix using R 4.2.1 and we sampled 100 pairs of the parameters d_V and V_0 on the basis of their uncertainty distribution using Simulx 2023R2 to compute the 95% confidence bands around predicted viral load curves.

As described in the Methods, we also tested whether age and/or sex should be included as covariates in our model estimates by performing correlation tests between these factors and the model estimates of d_V . These analyses suggested that age should be a covariate of the elimination rate d_V in the female and severe COVID-19 groups (t -statistic = -2.24 , P -value of 0.03 and t -statistic = -1.29 with P -value of 0.01, respectively), and sex should be retained in the estimation of d_V in the full cohort (t -statistic = -2.81 and P -value of 0.01). All other correlation tests indicated that both factors age and sex should be removed from the elimination rates in other subcohorts with P -value larger than 0.05. However, as the correlation test used the individual data rather than means within each subgroup, these t -statistics may introduce

inaccuracies because of the low number of data points for each patient. Thus, we ultimately opted not to include any covariates in our parameter estimates.

Our results showed that our simple viral dynamics model can reproduce the plasma vRNA dynamics of the entire population as well as each subgroup (Figure 3a–h). It is important to note that as we focussed on modelling plasma viral RNA loads and not viral production in the lungs, our model's predictions captured delays in the emergence of viral RNA in plasma.

In the full cohort, our results revealed a decline in plasma vRNA concentrations between the LOD and LOQ after DSO14, except for a noticeable increase in viral load at DSO22, which was particularly evident in critically ill and deceased patients (Figure 3f and h). Interestingly, the male subcohort showed marginally higher estimated viral concentrations with more variability than the female subcohort (Figure 3b and c). Regarding COVID-19 severity, our findings suggest that viral concentrations tended to be increased and exhibit more fluctuations with increasing disease severity. For example, critically ill patients exhibited the highest estimated plasma vRNA loads and the greatest variability. On the contrary, the viral kinetics of moderate patients showed slight variations between the LOD and LOQ after the first detected time point, whereas severely ill patients were predicted to have slightly higher viral loads, albeit with delayed recorded viral loads (Figure 3d–f). Lastly, survivors tended to have lower plasma vRNA concentrations that dipped below the LOQ after DSO14, while deceased patients exhibited relatively high and volatile viral loads that remained above the LOQ throughout our sampling period (Figure 3g and h). Together, these results support the observation that the rate of viral shedding (d_V) is a primary driver of differences in plasma SARS-CoV-2 RNA kinetics (Table 2).

Differences in SARS-CoV-2 RNA elimination kinetics distinguish COVID-19 severity

By comparing the viral dynamics of the subcohorts classified by patient sex, COVID-19 severity, and COVID-19 outcomes, we gained further insight into how each of these factors differentiated plasma vRNA kinetics. Our model predicted that female patients had lower peak viral loads and a

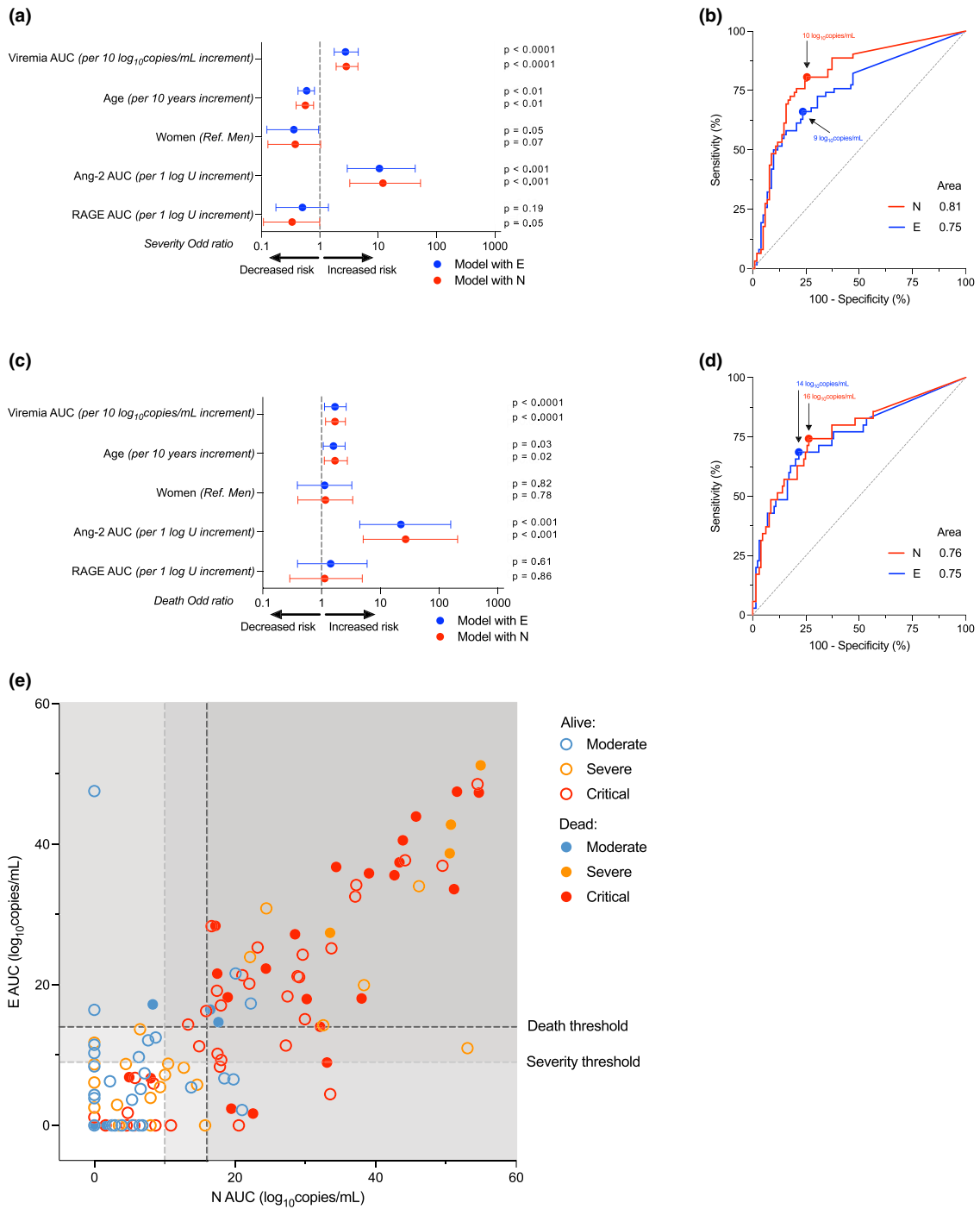


Figure 1. Relationships between plasma SARS-CoV-2 RNA probes, patient characteristics, and COVID-19 severity and outcomes. **(a)** Forest plot showing predictors (y-axis) of critical condition because of COVID-19 by logistic regression. Either measures of E (blue) or N (red) transcripts AUC were included in the model. Variables effects were estimated as log₁₀ of the odd ratios (x-axis). **(b)** ROC curves showing the ability of N and E transcripts AUC measures to predict severity. The thresholds of 9 and 10 log₁₀ copies/mL AUC for E and N, respectively, showed a high specificity in predicting severity. **(c)** Forest plot showing predictors (y-axis) of death because of COVID-19 by logistic regression. Either measures of E (blue) or N (red) transcripts AUC were included in the model. Variables effects are estimated as log₁₀ of the odd ratios (x-axis). **(d)** ROC curves showing the ability of N and E transcripts AUC measures to predict death. The thresholds of 14 and 16 log₁₀ copies/mL AUC for E and N, respectively, showed a high specificity in predicting death. **(e)** Correlation between E and N transcripts AUC according to severity (colours) and death (filled or open circles). Dotted line represents predictivity thresholds for death and severity. Undetectable viraemia during the period (AUC) are plotted at 0.

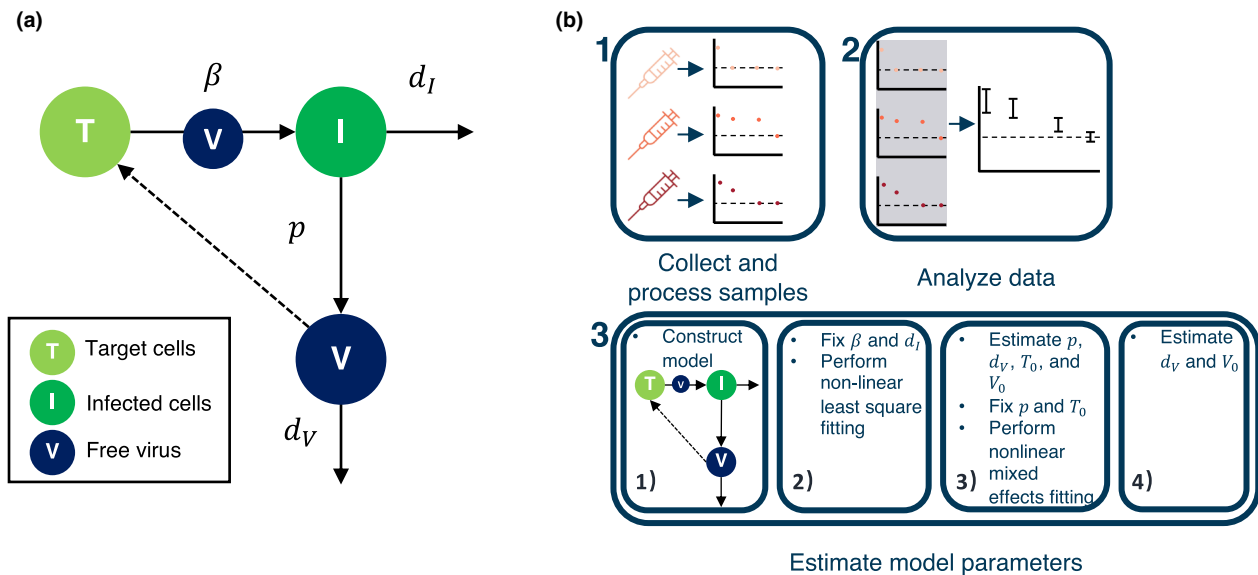


Figure 2. Graphical descriptions of model and parameter estimation workflow. **(a)** Target cell limited model (Equation 1) to predict the dynamics of target (T) and infected (I) cells and free virus (V). Target cells become infected at rate β to produce infected cells that die at rate d_I . Each infected cell releases p virions and dies at rate d_V . See [Methods](#) for complete model description. **(b)** Methodological approach to estimating viral clearance rates in hospitalised COVID-19 patients. **1.** Data were collected as described in the [Methods](#). Plasma vRNA loads below the limit of detection (LOD = 13 copies/mL) were set to 34 copies/mL i.e. half the limit of quantification (LOQ = 68 copies/mL) and measurements between 13 and 68 copies/mL were set to the LOQ (see [Methods](#)). **2.** Samples were separated into subgroups according to patient sex, disease severity and disease outcome. Data were then averaged in each subgroup and the full cohort at each day of symptom onset. **3.** Model parameters were then estimated as followed: **a.** Our model characterising the interactions among target cells, infected cells, and virus was developed (see panel 1). **2.** β and d_I were fixed to previously estimated values.¹³ **3.** p , d_V and T_0 were estimated using non-linear least squares and their values were fixed for the entire cohort. **4.** V_0 and d_V were then estimated in each subgroup using non-linear mixed-effects modelling.

plasma viral RNA clearance rate approximately 1.4-times higher than male patients (Figure 4a and Table 2). However, the 95% confidence bands overlapped, indicating that we could not statistically significantly distinguish the dynamics of viral elimination between male and female patients. Differences in SARS-CoV-2 RNA elimination rates were found to be pronounced when patients were grouped according to COVID-19 severity and outcomes. In the moderate group, plasma viral elimination was predicted to be about 1.5-fold higher than in the severe group whose elimination rate was approximately fourfold higher than in the critical group (Figure 4b and Table 2). Although higher initial viral inoculation was predicted for the moderate group, rapid viral elimination can effectively control viral concentrations in the host, driving down the viral load curve with lower maximum concentrations. As shown in Figure 4b, the confidence intervals around the three curves overlap before the maximum viral load is reached because of similar initial concentrations, whereas the significant differences in elimination rates make the viral

elimination patterns distinguishable thereafter. Plasma vRNA dynamics and viral clearance rates were particularly distinct when comparing COVID-19 survivors with those who did not survive the disease (Figure 4c). Among all cohorts, the deceased group was predicted to have the lowest initial viral concentrations and the slowest rate of viral clearance, all while demonstrating the highest degree of variability. Although the predicted viral load curve of deceased patients started from a low initial inoculum, its rapid acceleration caused it to surpass the viral load curve of the survivors and further extended their peak levels because of slow viral clearance. In contrast, the initial viral concentration of survivors was higher than that of nonsurvivors, and clearance rates were approximately 3.5-fold faster in COVID-19 survivors, resulting in an earlier peak with lower maximum viral concentrations and a more rapid decline in viral concentrations. This suggests that plasma SARS-CoV-2 RNA elimination kinetics can be used to establish the relationship between plasma vRNA concentrations and disease severity.

Table 1. Model parameters and estimates

Parameter	Description	Value (units)	Reference
β	Viral infectivity rate	0.18 (1/day \times 1/ log(copies/mL))	Jenner <i>et al.</i> (2021)
d_i	Rate of infected cell death	0.1 (1/day)	Jenner <i>et al.</i> (2021)
ρ	Lytic viral production rate	420 (1/day \times log (copies/mL))	Jenner <i>et al.</i> (2021)
d_v	Rate of plasma vRNA shedding	–	Fit (see Table 2)
$T(0)$	Initial number of target cells	1.27 (10^9 cells)	Fit
$I(0)$	Initial concentration of infected cells	0 (10^9 cells)	Fixed
$V(0)$	Initial plasma vRNA load	–	Fit (see Table 2)

Target-cell limited model parameters, their definitions and values. All fit parameters were estimated within the full cohort, except for d_v which was estimated within each subgroup (see [Methods](#) and [Table 2](#) for full results).

Plasma viral RNA loads are correlated with RAGE concentrations

As we found a link between the area under plasma SARS-CoV-2 RNA curve, and RAGE and Ang-2 AUC with severity ([Figure 1e](#)), we probed whether any relationship existed between the kinetics of predicted plasma vRNA loads and these two markers of lung tissue insult. We therefore quantified the correlation between plasma SARS-CoV-2 RNA, and RAGE and Ang-2 concentrations. In the full cohort, our results showed that average plasma SARS-CoV-2 loads were positively correlated with average RAGE concentrations at the 5% significance level ([Table 3](#), [Figure 5](#) for the full cohort and COVID-19 severity, and [Supplementary figure 2](#) for the results according to sex and COVID-19 outcome), whereas no relationship was found between plasma vRNA loads and Ang-2 in the full cohort or in any subgroup (see [Supplementary table 3](#) and [Supplementary figure 3](#)).

The strongest correlation was found between RAGE and plasma SARS-CoV-2 RNA in the severe subgroup, with a correlation of 0.78 (P -value of 1.00×10^{-3}). We also found a strong association between viral load and RAGE levels in the critical group and among male patients, with correlation coefficients of around 0.7 (P -values < 0.05). This relationship was found to be moderate in survivors ($r = 0.46$, P -value = 7.03×10^{-2}), while no significant relationship was found between

average SARS-CoV-2 RNA loads and RAGE concentrations in the moderate and deceased groups. These results reveal important insights into the mechanisms underlying COVID-19 pathogenesis and the potential use of RAGE as a prognostic biomarker in severe and critical cases.

By appropriately adjusting RAGE levels to match plasma vRNA load ranges, we visualised their correlations by comparing RAGE levels over time *versus* predicted viral load curves for the entire cohort as well as for each subgroup ([Figure 5](#) and [Supplementary figure 2](#)). In the full cohort, our results showed that RAGE concentrations in the first 20 days after symptom onset exhibited similar elimination rates to predicted plasma vRNA loads, but that they remained elevated beyond DSO20, decreasing the measured correlation between plasma vRNA and RAGE concentrations over the full 30 days considered in our analyses ([Figure 5a](#)). This pattern was particularly pronounced in the moderate group ([Figure 5b](#)), resulting in the lowest correlation between vRNA and RAGE. In contrast, mean RAGE concentrations in the severe and critical groups were found to be highly correlated with predicted plasma vRNA curves throughout the first 30 days after symptom onset ([Figure 5c and d](#)).

DISCUSSION

Establishing the factors affecting the pathophysiology driving COVID-19 severity is of high clinical importance.⁵ We have previously reported that plasma vRNA concentrations at fixed days after symptom onset are an early predictor of COVID-19 mortality.¹² Here, we used mathematical modelling based on serial plasma viral RNA measurements from hospitalised patients to establish differences in plasma vRNA kinetics within patient subgroups characterised according to patient sex, COVID-19 severity and disease outcome.

We first evaluated whether SARS-CoV-2 plasma viraemia could predict severity and death. Using sequential measures of viraemia, we calculated AUC for both N and E transcripts and confirmed the strong correlation between these two measures, as we previously reported.¹² AUC viraemia efficiently predicted COVID-19 outcome, with a fourfold increased risk in severity and a fivefold increased risk of death when AUC viraemia was above the defined thresholds. These results add to the growing body of literature

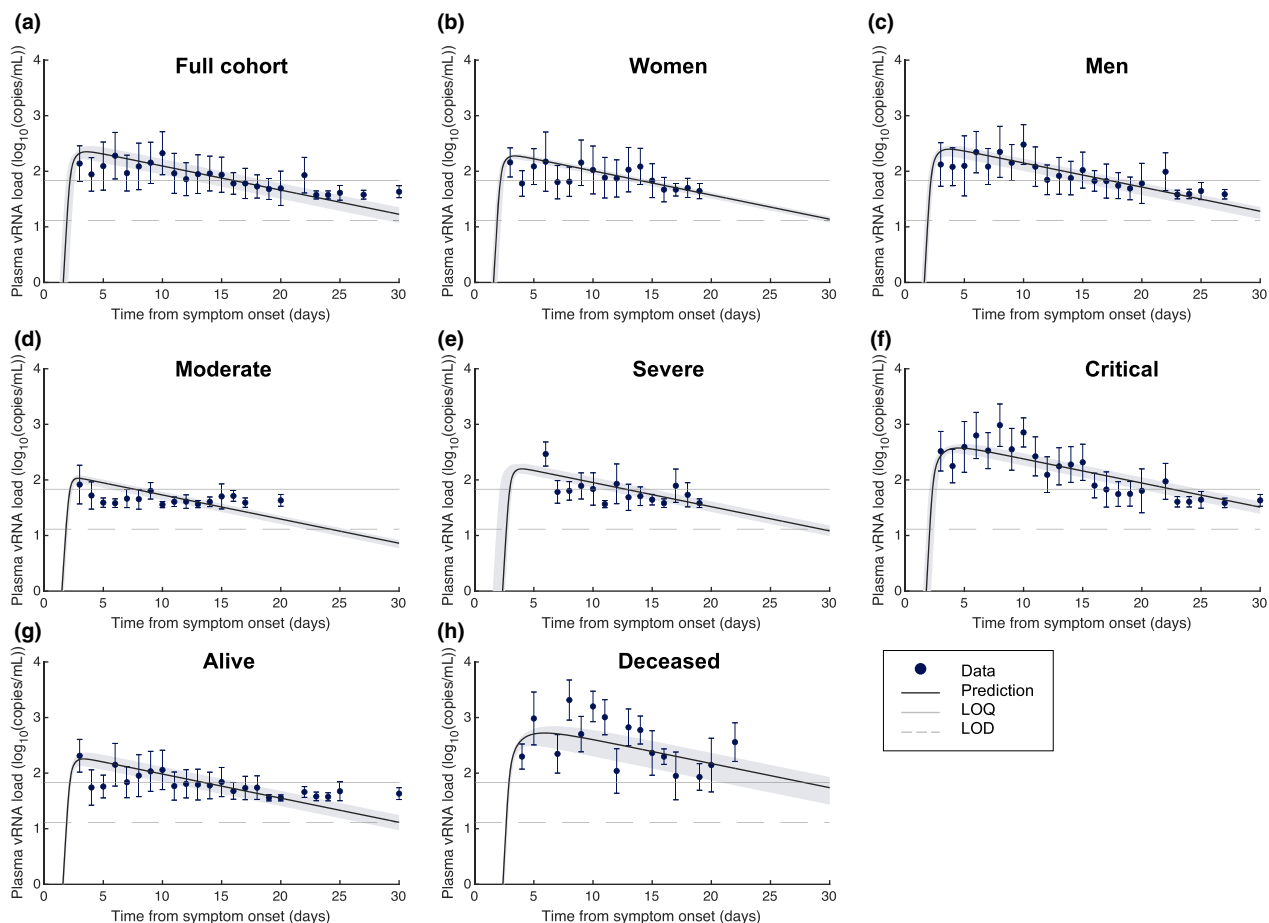


Figure 3. Mathematical model predicts plasma vRNA dynamics in hospitalised COVID-19 patients. Plasma vRNA kinetics predicted by fitting a basic viral dynamics model (Equation 1) and estimating initial viral loads ($V(0)$) and viral clearance rates (d_v) using non-linear mixed-effects modelling in (a) the full cohort, (b) female patients, (c) male patients, (d) the moderate patient group, (e) the severe patient group, (f) critical patients, (g) survivors and (h) deceased patients. (a–h) Solid lines, model-predicted vRNA concentrations using population parameters; error bars, standard errors of the mean (calculated from the raw data) at each time point; dashed dark grey line, level of quantification (LOQ). Dashed light grey line, level of detection (LOD). The coloured areas are the confidence bands for each predicted viral load curve.

Table 2. Plasma vRNA shedding rates distinguish COVID-19 severity in hospitalised patients

Group	Initial viral load (V_0 , log(copies/mL))	95% CI of V_0	Viral decay rate (d_v , (1/day))	95% CI of d_v
Full cohort	1.47×10^{-6}	$[4.06 \times 10^{-7}, 5.30 \times 10^{-6}]$	2.01	[1.79, 2.26]
Female	2.43×10^{-6}	$[5.13 \times 10^{-7}, 1.15 \times 10^{-5}]$	2.48	[2.07, 2.97]
Male	1.14×10^{-6}	$[2.46 \times 10^{-7}, 5.27 \times 10^{-5}]$	1.74	[1.49, 2.03]
Moderate	2.14×10^{-5}	$[7.67 \times 10^{-6}, 5.95 \times 10^{-5}]$	4.50	[4.03, 5.03]
Severe	4.18×10^{-9}	$[5.72 \times 10^{-10}, 3.06 \times 10^{-8}]$	2.96	[2.43, 3.60]
Critical	1.82×10^{-7}	$[7.65 \times 10^{-9}, 4.33 \times 10^{-6}]$	1.12	[0.84, 1.51]
Alive	2.88×10^{-6}	$[8.43 \times 10^{-7}, 9.83 \times 10^{-6}]$	2.55	[2.29, 2.84]
Deceased	9.24×10^{-10}	$[1.02 \times 10^{-10}, 8.39 \times 10^{-9}]$	0.74	[0.54, 1.02]

Plasma viral RNA elimination kinetics were estimated within subgroups defined by sex, disease severity and disease outcome using a non-linear mixed-effects model. We estimated distinct differences in d_v values according to patient sex and COVID-19 severity. Notably, a large decrease in viral shedding rates was observed between survivors and nonsurvivors. Shading distinguishes segregating subgroups (e.g. female and male).

indicating that detectable levels of SARS-CoV-2 transcripts in plasma are associated with COVID-19 severity.^{4,31–34} Recent studies reported that

infectious virus is usually not recovered from the plasma of viraemic SARS-CoV-2 infected individuals,^{31,35} suggesting that detection of viral

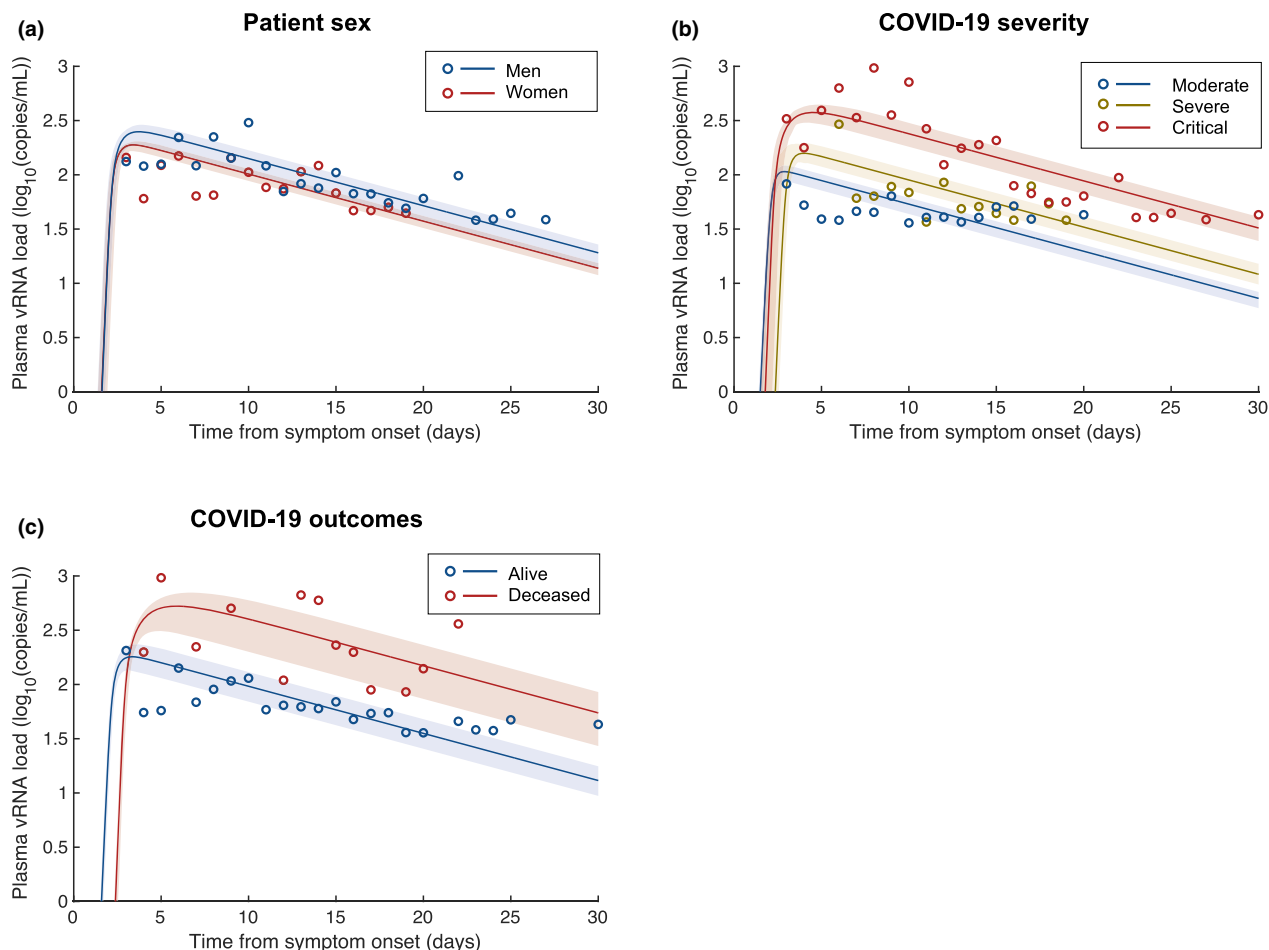


Figure 4. COVID-19 severity is characterised by differences in plasma vRNA clearance rates. Plasma vRNA kinetics predicted by fitting our basic viral dynamics model (Equation 1) and estimating viral clearance rates (d_v) according to patient sex, COVID-19 severity and disease outcomes. Predicted and observed viral loads for (a) female and male patients, (b) patients grouped according to COVID-19 severity and (c) survivors and deceased patients. (a–c) Solid lines: predicted plasma vRNA concentrations. The coloured areas are the confidence bands for each predicted viral load curve. The solid circles indicate the average viral concentrations at each DSO for the corresponding groups.

Table 3. Correlation between average plasma vRNA and RAGE concentrations

Group	Pearson's correlation	P-value
Full cohort	0.63	1.10×10^{-3}
Female	0.62	8.20×10^{-3}
Male	0.72	1.10×10^{-4}
Moderate	0.46	7.03×10^{-2}
Severe	0.78	1.00×10^{-3}
Critical	0.68	2.20×10^{-4}
Alive	0.54	7.30×10^{-3}
Deceased	0.37	1.63×10^{-1}

Average plasma viral RNA and RAGE were calculated within subgroups defined by sex, disease severity and disease outcome for each DSO. Correlation coefficients were calculated based on average plasma viral load and RAGE concentrations at each DSO (see Methods). The corresponding results for Ang-2 are provided in Supplementary table 3. Shading distinguishes segregating subgroups (e.g. female and male).

RNA in plasma likely results from the translocation of viral products from the lungs into the blood, rather than from the systemic replication of SARS-CoV-2. Hence, single viral load measures, but more importantly, total exposure as measured by AUC in our study, are likely to reflect the degree of lung insult, which may explain their positive predictive values for disease severity.

In support of this model, by examining the relationships between plasma viral RNA concentrations and two immunological markers of lung tissue insult, we found a positive correlation between plasma viral load and RAGE concentrations. In particular, RAGE levels were strongly correlated with plasma vRNA concentrations and viral kinetics in the severe and critical subgroups. In contrast to our AUC results

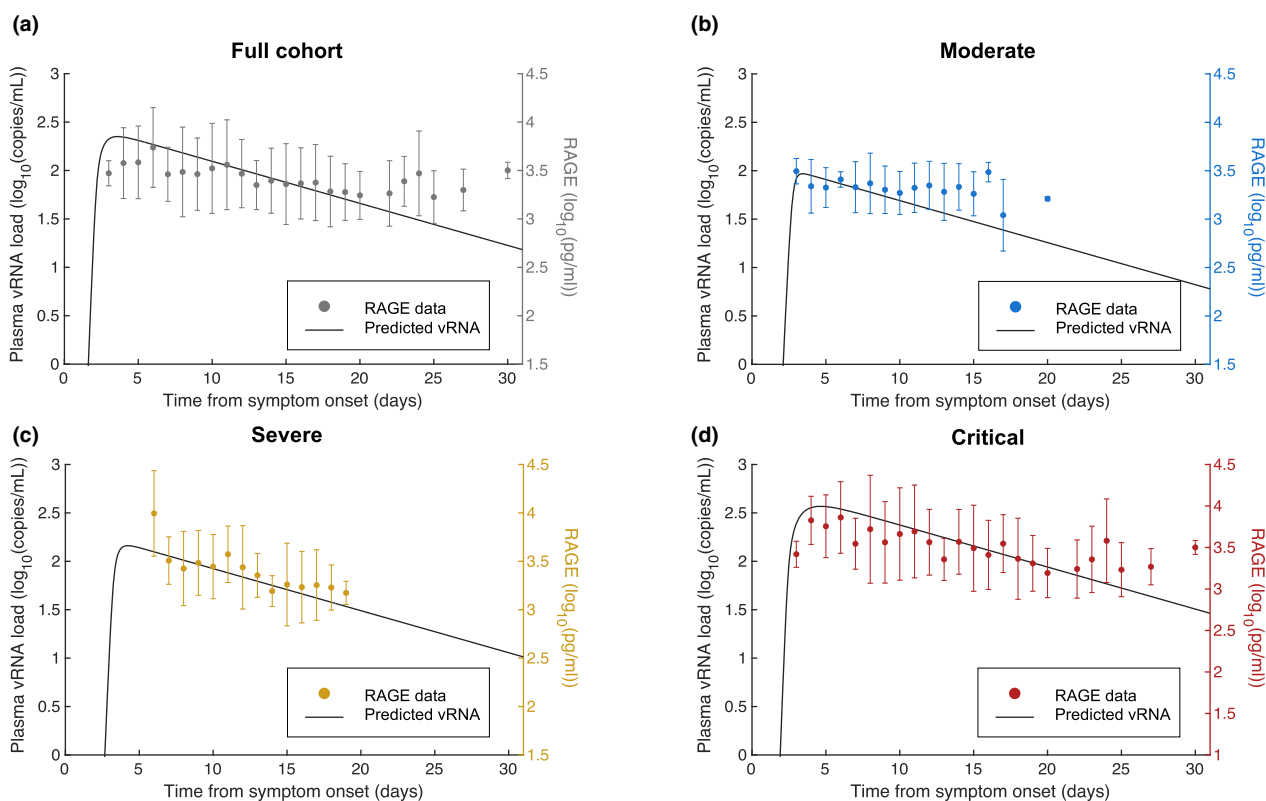


Figure 5. Average RAGE concentrations are positively correlated with average plasma vRNA loads. Average RAGE concentrations were found to be associated to predicted plasma viral loads. Viral load and RAGE concentrations for **(a)** the entire cohort, **(b)** the moderate patient group, **(c)** severe patients and **(d)** the critical group. **(a–d)** Solid lines: predicted plasma vRNA concentrations. Dots: average RAGE data derived from clinical data. Error bars: standard error at each time point calculated from the raw data.

(Figure 1), we found no correlation between Ang-2 concentrations and vRNA AUC. While both RAGE and Ang-2 are markers of lung tissue insult, they relate to different damages: RAGE is associated with acute alveolar epithelial injury while Ang-2 relates to endothelial damage. Our model suggests that the source of plasma vRNA more likely stems from a breach of the alveoli rather than of the blood vessels supplying them. This also suggests a link between the higher risk associated with plasma viraemia and the high expression of emergency pathways of alveolar regeneration expressed in autopsied lungs post-COVID.¹¹

By comparing the estimated viral shedding patterns of the entire cohort and the cohort subgroups, our results indicated that viral clearance rates drove heterogeneous viral dynamics. Moreover, plasma viral kinetics, and particularly the plasma vRNA elimination rate, were predicted to differ depending largely on severity and outcome of COVID-19. Notably, increases in severity and mortality were found to be accompanied by a significant decrease in viral

clearance rate and higher peak viral loads. More specifically, in severe patients, viral clearance dropped to one-fourth that of moderate patients. Furthermore, viral clearance was more than three times faster in survivors than in deceased patients. Interestingly, female patients were found to have higher plasma viral elimination rates than male patients, which may be one mechanism behind lesser severities seen in women. Taken together, our results suggest that plasma viral RNA kinetics, and particularly the rate of viral shedding, is associated with COVID-19 severity. Furthermore, given the connection between RAGE and plasma SARS-CoV-2 kinetics (Figure 5), RAGE could be used as a proxy measure for the plasma kinetics of SARS-CoV-2 RNA concentrations to prospectively evaluate COVID-19 severity.

A limitation of our study is the use of average plasma vRNA per day of symptom onset to estimate viral dynamics and shedding rates within each subgroup. This approach is simple to obtain but is insufficient to fully characterise dispersion within the data and may be affected by data sparsity,

especially for DSOs with few patient observations (e.g. less than three). Alternative approaches could include bootstrapping to artificially densify data and fitting multiple replicate samples using non-linear mixed-effects models. This can be very computationally taxing and introduces additional noise, so we opted here to instead work directly with the raw data. Furthermore, although our approach to undetectable and unquantifiable plasma vRNA data reduced data information loss, it slightly increased average viral loads and decreased the standard deviation per DSO. Moreover, our target-cell limited model only described the temporal relationship between target cells, infected cells and SARS-CoV-2 virus without considering the impact of antibodies and immune responses. Future work should consider variables that are highly correlated with disease severity (see, for example, Jenner *et al.* 2021¹³) to provide a more comprehensive picture of their interactions with plasma vRNA shedding rates.

Our analyses provide further strong evidence that viral clearance rates distinguish COVID-19 severity,²² which is critical for identifying at-risk populations. Our results suggest that treatments acting to accelerate viral clearance as part of a multidimensional therapeutic approach may provide benefit to hospitalised patients if administered before DSO 4 according to the predicted plasma vRNA load curve of the moderate group. Furthermore, our model's predictions support early and serial testing of plasma vRNA loads to better assess the likelihood of COVID-19 severity. Importantly, our results support the use of more easily obtainable RAGE concentrations as a suitable surrogate of plasma viral load to distinguish severe COVID-19 patients. This study demonstrates the importance of assessing immunovirological dynamics in COVID-19 and the role of mathematical modelling to quantify key drivers of these kinetics.

METHODS

Study cohort and cohort subgroups

As described previously,¹² our cohort includes individuals with symptomatic infection and a positive SARS-CoV-2 nasopharyngeal swab PCR hospitalised with COVID-19 at either the Centre Hospitalier de l'Université de Montréal (CHUM) or the Jewish General Hospital (JGH) in Montréal, Canada and enrolled in to the Québec COVID-19 biobank.³⁶ Samples were collected at recruitment into the full cohort and at hospitals days 0, 2, 7, 14 and 30. Samples were

collected if blood was otherwise required for clinical purposes within a 48-h window of the requested time points. Following discharge, follow-up visits were planned at days 30, 90, 180, 365, 545 and 760. COVID-19 severity (i.e. moderate, no oxygen support; severe, oxygen support with low flow nasal cannula; or critical, requiring oxygenation by high flow nasal cannula, non-invasive or invasive mechanical ventilation) was assessed over the course of hospital stay. Fatal outcomes were any deaths which occurred within 60 days of symptom onset (DSO60).

To study differences in plasma vRNA kinetics according to patient-specific characteristics, we established seven different nonexclusive subgroups in addition to the full cohort. We grouped patients based on traits including sex (male and female), maximum severity (moderate, severe and critical) and outcomes at DSO60 (alive and deceased). Total patient numbers in each group are reported in Table 4.

Quantification of plasma viral RNA

Absolute copy numbers of SARS-CoV-2 RNA (N and E regions) in plasma samples were measured by real-time PCR. Viral RNAs were extracted from 230 μ L of plasma collected on EDTA using the QIAamp Viral RNA Mini Kit (Qiagen, Germantown, Maryland, USA, Cat. No. 52906), according to the manufacturer's instructions. Real-time PCRs were performed in 384-well plates using the TaqPath 1-Step Multiplex Master Mix (No ROX) (Thermo Fischer Scientific, Frederick, Maryland, USA, Applied Biosystems Cat. No. A28521) on a QuantStudio 5 instrument. Three master reaction mixes with specific primers and probes were prepared for quantification of N and E genes from SARS-CoV-2 and 18S (as a control for efficient extraction and amplification). The RT-qPCR was performed in a volume of 15 μ L including 3.75 μ L of Taqpath Master Mix, 1.88 μ L of an 8 \times mix of primers/probe (providing a final concentration of each primer of 400 nM (N and 18S) or 800 nM (E) and probe of

Table 4. Full cohort and patient subgroups

Subgroup	Total number of patients	Percentage of full cohort (%)	Number of viraemic patients	Percentage of full cohort (%)
Full cohort	294	100	256	87
Female	127	43	117	46
Male	166	57	139	54
Moderate COVID-19	94	32	80	31
Severe COVID-19	87	30	77	30
Critical COVID-19	112	38	99	39
Alive	246	84	212	83
Deceased	47	16	44	17

Plasma SARS-CoV-2 RNA kinetics were analysed in eight different subgroups according to sex, COVID-19 severity and outcomes at DSO60. Shading indicates segregating subgroups (e.g. female and male).

200 nM), 4.38 μL of H_2O and 5 μL of the RNA extracts, controls or standards. The cycling parameters for qPCR were 53°C for 10 min, 95°C for 2 min and then 95°C for 3 s and 60°C for 30 s for 45 cycles. N and E SARS-CoV-2 quantifications were performed in quadruplicate and 185 measurements were performed in duplicates. The sequences of the primers and probes are provided in Supplementary table 1. Positive and no-template controls were included in all experiments.

To obtain absolute copy numbers of N and E SARS-CoV-2 transcripts, *in vitro* transcribed RNA standards were generated. Linear DNA templates for *in vitro* transcription containing a T7 promoter upstream of the complete sequence of N or E genes were generated by PCR from a commercially available plasmid (Integrated DNA Technologies, Coralville, Iowa, USA, 2019-nCoV-N_positive plasmid – IDT Cat. No. 10006625; 2019-nCoV-E_positive plasmid – IDT Cat. No. 10006896). The PCR reaction was performed in a total volume of 50 μL : 0.5 μL of Taq Polymerase (Thermo Fischer Scientific, Frederick, Maryland, USA, Invitrogen Cat. No. 18038042), 5 μL of 10 \times Reaction Mix, 3 μL of MgCl_2 (50 mM), 1.5 μL of dNTP (10 mM), 2.5 μL of each primer (10 μM , providing a final concentration of each primer of 500 nM), 25 μL of H_2O and 10 μL of the plasmid. The sequences of the primers are given in Supplementary table 2.

The cycling parameters were 94°C for 3 min and then 94°C for 45 s, 55°C 30 s and 72°C for 2 min for 40 cycles of amplification, with a final extension at 72°C for 10 min. The PCR product was purified using the QIAquick PCR purification kit according to the manufacturer's protocol (Qiagen, Germantown, Maryland, USA, Cat. No. 28104). RNA transcripts were produced *in vitro* using the MEGAscript T7 Transcription Kit (Thermo Fischer Scientific, Frederick, Maryland, USA, Invitrogen Cat. No. AM1333). The transcription reaction was performed in a total volume of 20 μL : 2 μL of 10 \times Reaction Buffer, 2 μL of each rNTP, 2 μL of Enzyme Mix and 0.5–2 pmol M13-flanked DNA template. The reaction was performed at 37°C for 4 h, then 1 μL of TURBO DNase was added and incubated for an additional 15 min at 37°C. RNA transcripts were then purified using the RNeasy mini kit according to the manufacturer's protocol (Qiagen, Germantown, Maryland, USA, Cat. No. 74104). Purified RNA N and E transcripts (1328 nt for N and 296 nt for E) were quantified by Nanodrop and the RNA copy numbers were calculated using the ENDMEMO online tool (<http://www.endmemo.com/bio/dnacopynum.php>). Aliquots of 10^{11} copies/ μL were stored at -80°C . For each qPCR batch, one aliquot was thawed, and six serial dilutions were prepared to generate a standard curve (500 000 to 5 RNA copies per PCR well).

Quantification of RAGE and Ang-2 concentrations by Luminex

Never-thawed plasma aliquots were thawed at RT and SARS-CoV-2 virus was inactivated using 1% Triton-X100 for 2 h at RT. After inactivation, measurements were taken in duplicates using a customised Human Magnetix Luminex Assay (LXSAHM-26), as per the manufacturer's instructions. Plates were acquired using a Bio-plex 200 array system (Bio-Rad Laboratories) for CHUM samples, or MagPix[®] System (Luminex) for samples from JGH. Raw fluorescence intensity

values were first manually background-subtracted, then concentrations were extrapolated using each plate's individual standard curve for all analytes using the *bcrn* package in R to construct a Bayesian Continual Reassessment Method model.³⁷

Area under the curve (AUC) analysis

To analyse the kinetics of SARS-CoV-2 plasma viraemia and reflect its levels over the course of the disease, we calculated the viraemia AUC for both N and E transcripts. For this analysis, we selected participants with at least two RNA measurements available between DSO0 and DSO30, and at least one measurement between DSO6 and DSO16 (which was previously identified as the period during which plasma viraemia peaks¹²). For all participants, DSO0 and DSO30 were artificially set at threshold (limit of detection: 0.81 \log_{10} copies/mL), since SARS-CoV-2 RNA was not detected in any sample collected at these dates. N or E AUC were thus inferred in two different logistic regression model to predict outcome (severity and death), along with other previously identified clinical (age and sex) and biological (Ang-2 and RAGE) parameters.

Determining the association between viral kinetics and lung tissue insult markers

To investigate the association between lung tissue insult markers and plasma vRNA kinetics, we assessed the correlation between viral load and each marker from DSO0 to DSO30. For this, we first transformed RAGE and angiotensin-2 (Ang-2) concentrations to the \log_{10} scale and then calculated the mean and standard deviation at each DSO for the entire cohort and each subcohort, as described above. Pearson's correlation coefficients and *P*-values between RAGE and Ang-2 and plasma viral RNA concentrations were then quantified using the *corr* function in Matlab r2022a.³⁸

Mathematical model of plasma SARS-CoV-2 kinetics

To predict plasma vRNA concentrations in the full cohort and each subgroup, we applied the target cell-limited model.³⁹ This model is a system of ordinary differential equations describing the temporal evolution of target (*T*) and infected cells (*I*) and free virus (*V*) (Figure 2a) given by

$$\frac{dT}{dt} = -\beta TV,$$

$$\frac{dI}{dt} = \beta TV - d_I I,$$

$$\frac{dV}{dt} = pI - d_V V. \quad (1)$$

Here, target cells interact with free SARS-CoV-2 particles and become infected at rate β , infected cells produce p

virions per cell and die at rate d_i , and free virus is cleared at rate d_v .

We have previously successfully applied a similar model to predict viral loads from nasopharyngeal (NP) samples¹³ that are typically orders of magnitude higher than plasma vRNA titres. Supplementary figure 1 demonstrates the ability of the model in Equation 1 and Methods described herein to characterise NP viral loads from hospitalised patients. The focus of this study was to apply this model to plasma vRNA concentrations to determine their dynamics and association with COVID-19 biomarkers and outcomes.

Data processing and model parameter estimation

To estimate our model's parameters, we restricted our analysis to a period between 0- and 30-day postsymptom onset (DSO). To reduce the possibility of overestimating viraemia before 6 or after 20 DSO, viral load measurements below the limit of detection (LOD = 13 copies/mL) were set to 34 copies/mL, that is half the limit of quantification (LOQ = 68 copies/mL),⁴⁰ and measurements between 13 and 68 copies/mL were set to the LOQ. One severely immunocompromised patient (male organ transplant recipient) was removed from the analysis as an outlier after observing persistently high vRNA loads that were inconsistent with the rest of the cohort. Patients were then assigned to the subgroups described in Table 4. For each subgroup, we calculated the mean and standard deviation of plasma viral load (in \log_{10} copies/mL) each day postsymptom onset. DSOs with only one patient observation were removed to avoid standard deviations of 0.

Based on our previous work,¹³ we first fixed the initial concentration of infected cells (I_0), the decay rate of infected cells (d_i) and rate of infectivity (β). We chose to refit the number of initial number target cells (T_0), as our earlier work focussed on viral load dynamics in the lungs.

Next, to determine the viral kinetic parameters that demonstrated the most heterogeneity between cohort subgroups, we first fit average the plasma vRNA concentrations in each subgroup using non-linear least squares by minimising the squared difference between observed and predicted average plasma vRNA loads, i.e.

$$\min\left(\sum_{i=1}^n \|V(t_{ij}) - Y_{ij}\|^2\right),$$

using the function *lsqnonlin* in Matlab. In the equation above, Y_{ij} denotes the average observed plasma vRNA of subgroup i at time t_{ij} (in \log_{10} copies/mL) and $V(t_{ij})$ is the predicted viral load at time t_{ij} . Each parameter was initialised to values estimated in our previous work.¹³

From this initial analysis, we determined that only the rate of viral elimination (d_v) differed drastically between subgroups, with smaller differences observed in initial viral loads (V_0). Thus, to better quantify the degree of heterogeneity in this key parameter between each subgroup, we fixed all other model parameters¹³ and fit only d_v and V_0 using a non-linear mixed-effects model in Monolix,⁴¹ as in previous studies.^{22,42}

We fitted the structural model

$$Y_{ij} = \log_{10} V(t_{ij}, \Psi_{ij}) + e_{ij},$$

as in Néant et al.²² Here Ψ_{ij} is the vector parameters of subgroup i , with each parameter Ψ_i taken to be log-normally distributed according to

$$\Psi_i = \theta_i e^{\eta_i}$$

with θ_i the fixed effect and η_i the random effect. Similar to the non-linear least-squares equation above, $V(t_{ij}, \Psi_{ij})$ represents the predicted viral load from Equation (1) and e_{ij} is a normally distributed additive error term with mean 0 and standard deviation σ_{ij} (i.e. $e_{ij} \sim N(0, \sigma_{ij})$). We also explored the inclusion of covariates for sex and age in our model parameter estimates by performing the correlation test in Monolix between each factor and the elimination rate d_v for each group. For this, Monolix implements a linear regression between the covariates and d_v to test whether the estimated beta coefficients are statistically significantly different from 0 using a Student's *t*-test. A schematic description of the data analysis and parameter estimation workflow is provided in Figure 2b.

ACKNOWLEDGMENTS

We thank all the patients, family members and staff from all the units who participated in the study. While we cannot thank everyone personally, we thank the teams of Drs Madeleine Durand, Michaël Chassé, Brent Richards, Daniel Kaufmann and technicians from other laboratories at the CRCHUM for patient recruitment, sample collection and blood specimen processing. We also thank the clinical research teams for clinical data retrieval, and J Plantin, C Dufour, I Turcotte and R Fromentin for sample collection and processing. We also acknowledge the help of Marc Messier Peet, Pascale Arlotto, Nakome Nguissan, Fatma Mayil, Maya Salame and Nathalie Brassard for participant recruitment at CHUM.

AUTHOR CONTRIBUTIONS

Xiaoyan Deng, Pierre Gantner, Julia Forestell, Amélie Pagliuzza, Elsa Brunet-Ratnasingham, Madeline Durand, Daniel E Kaufmann, Nicolas Chomont and Morgan Craig were involved in conceptualisation. Xiaoyan Deng, Pierre Gantner, Julia Forestell, Amélie Pagliuzza, Madeline Durand, Daniel E Kaufmann, Nicolas Chomont and Morgan Craig were involved in data curation. Xiaoyan Deng, Pierre Gantner, Julia Forestell, Amélie Pagliuzza, Elsa Brunet-Ratnasingham, Madeline Durand, Daniel E Kaufmann, Nicolas Chomont and Morgan Craig were involved in formal analysis. Daniel E Kaufmann, Nicolas Chomont and Morgan Craig were involved in funding acquisition and supervision. Xiaoyan Deng, Pierre Gantner, Julia Forestell, Amélie Pagliuzza, Elsa Brunet-Ratnasingham, Madeline Durand, Daniel E Kaufmann, Nicolas Chomont and Morgan Craig were involved in investigation. Xiaoyan Deng, Pierre Gantner, Daniel E Kaufmann, Nicolas Chomont and Morgan Craig were involved in methodology. Xiaoyan Deng, Pierre Gantner and Morgan Craig were involved in writing—original draft. Xiaoyan Deng, Pierre Gantner, Julia Forestell, Amélie Pagliuzza, Elsa Brunet-Ratnasingham, Madeline Durand, Daniel E Kaufmann, Nicolas Chomont and Morgan Craig were involved in writing—review & editing.

FUNDING

American Foundation for AIDS Research (amfAR) grant 110068-68-RGCV (DEK, NC), Canada's COVID-19 Immunity Task Force (CITF), in collaboration with the Canadian Institutes of Health Research (CIHR) grant VR2-173203 (DEK), CRCHUM Foundation and Foundation du CHUSJ. The Biobanque québécoise de la COVID-19 (BQC19) is funded by the FRQS, Génome Québec and the Public Health Agency of Canada. MD is a FRQS J2 Clinician researcher Scholar. EBR is recipient of a COVID-19 excellence scholarship from the Université de Montréal. Natural Sciences and Engineering Research Council of Canada Discovery Grant RGPIN-2018-04546, COVID-19 Alliance Grant ALLRP 554923-20, and NSERC Emerging Infectious Disease Modelling Network Grant to the One Health Modelling Network for Emerging Infections (XD, MC). DEK is a FRQS Merit Research Scholar. NC is a FRQS Senior Research Scholar. MC is a FRQS J1 Research Scholar.

CONFLICT OF INTEREST

The authors declare no conflict of interest.

DATA AVAILABILITY STATEMENT

All data needed to evaluate the conclusions in the paper are present in the paper and/or the Supplementary Materials. Code is available on Github (<https://github.com/dengxy92/Plasma-vRNA-COVID-19-Severity.git>).

REFERENCES

1. Arunachalam PS, Wimmers F, Mok CKP *et al.* Systems biological assessment of immunity to mild versus severe COVID-19 infection in humans. *Science* 2020; **369**: 1210–1220.
2. Bermejo-Martin JF, González-Rivera M, Almansa R *et al.* Viral RNA load in plasma is associated with critical illness and a dysregulated host response in COVID-19. *Crit Care* 2020; **24**: 691.
3. Silva J, Lucas C, Sundaram M *et al.* Saliva viral load is a dynamic unifying correlate of COVID-19 severity and mortality. *Infectious Diseases (except HIV/AIDS)*, 2021 <https://doi.org/10.1101/2021.01.04.21249236>
4. Fajnzylber J, Regan J, Coxen K *et al.* SARS-CoV-2 viral load is associated with increased disease severity and mortality. *Nat Commun* 2020; **11**: 5493.
5. Lucas C, Wong P, Klein J *et al.* Longitudinal analyses reveal immunological misfiring in severe COVID-19. *Nature* 2020; **584**: 463–469.
6. Park A, Iwasaki A. Type I and type III interferons – Induction, signaling, evasion, and application to combat COVID-19. *Cell Host Microbe* 2020; **27**: 870–878.
7. Puchinger K, Castelletti N, Rubio-Acero R *et al.* The interplay of viral loads, clinical presentation, and serological responses in SARS-CoV-2 – Results from a prospective cohort of outpatient COVID-19 cases. *Virology* 2022; **569**: 37–43.
8. Gomez Marti JL, Mays A, McCullough M, Wells A, Phan T. Evaluation of viral loads in patients with SARS-CoV-2 Delta variant infection: Higher loads do not translate into different testing scenarios. *Microbiol Insights* 2022; **15**: 117863612210875.
9. Blot M, Jacquier M, Manoha C *et al.* Alveolar SARS-CoV-2 viral load is tightly correlated with severity in COVID-19 ARDS. *Clin Infect Dis* 2021; **72**: e446–e447.
10. Mestdagh P, Gillard M, Dhillon SK *et al.* Evaluating diagnostic accuracy of saliva sampling methods for severe acute respiratory syndrome coronavirus 2 reveals differential sensitivity and association with viral load. *J Mol Diagn* 2021; **23**: 1249–1258.
11. Hirschbühl K, Schaller T, Märkl B *et al.* High viral loads: What drives fatal cases of COVID-19 in vaccinees? – An autopsy study. *Mod Pathol* 2022; **35**: 1013–1021.
12. Brunet-Ratnasingham E, Anand SP, Gantner P *et al.* Integrated immunovirological profiling validates plasma SARS-CoV-2 RNA as an early predictor of COVID-19 mortality. *Sci Adv* 2021; **7**: eabj5629.
13. Jenner AL, Aogo RA, Alfonso S *et al.* COVID-19 virtual patient cohort suggests immune mechanisms driving disease outcomes. *PLoS Pathog* 2021; **17**: e1009753.
14. Farhang-Sardroodi S, Korosec CS, Gholami S *et al.* Analysis of host immunological response of adenovirus-based COVID-19 vaccines. *Vaccines* 2021; **9**: 861.
15. Korosec CS, Farhang-Sardroodi S, Dick DW *et al.* Long-term predictions of humoral immunity after two doses of BNT162b2 and mRNA-1273 vaccines based on dosage, age and sex. *Infectious Diseases (except HIV/AIDS)*, 2021. <https://doi.org/10.1101/2021.10.13.21264957>
16. Baccam P, Beauchemin C, Macken CA, Hayden FG, Perelson AS. Kinetics of influenza a virus infection in humans. *J Virol* 2006; **80**: 7590–7599.
17. Smith AM. Host-pathogen kinetics during influenza infection and coinfection: Insights from predictive modeling. *Immunol Rev* 2018; **285**: 97–112.
18. Smith AM, Perelson AS. Influenza a virus infection kinetics: Quantitative data and models. *WIREs Syst Biol Med* 2011; **3**: 429–445.
19. Smith AP, Moquin DJ, Bernhauerova V, Smith AM. Influenza virus infection model with density dependence supports biphasic viral decay. *Front Microbiol* 2018; **9**: 1554.
20. Bankhead A, Mancini E, Sims AC, Baric RS, McWeeney S, Sloot PMA. A simulation framework to investigate in vitro viral infection dynamics. *Procedia Comput Sci* 2011; **4**: 1798–1807.
21. Korell J, Green B, DeVincenzo J, Huntjens D. A human challenge model for respiratory syncytial virus kinetics, the pharmacological effect of a novel fusion inhibitor, and the modelling of symptoms scores. *Eur J Pharm Sci* 2017; **109**: S154–S160.
22. Néant N, Lingas G, Le Hingrat Q *et al.* Modeling SARS-CoV-2 viral kinetics and association with mortality in hospitalized patients from the French COVID cohort. *Proc Natl Acad Sci USA* 2021; **118**: e2017962118.
23. Kim KS, Ejima K, Iwanami S *et al.* A quantitative model used to compare within-host SARS-CoV-2, MERS-CoV, and SARS-CoV dynamics provides insights into the pathogenesis and treatment of SARS-CoV-2. *PLoS Biol* 2021; **19**: e3001128.

24. Goyal A, Cardozo-Ojeda EF, Schiffer JT. Potency and timing of antiviral therapy as determinants of duration of SARS-CoV-2 shedding and intensity of inflammatory response. *Sci Adv* 2020; **6**: eabc7112.
25. Perelson AS, Ke R. Mechanistic modeling of SARS-CoV-2 and other infectious diseases and the effects of therapeutics. *Clin Pharmacol Ther* 2021; **109**: 829–840.
26. Matthay MA, Zemans RL, Zimmerman GA et al. Acute respiratory distress syndrome. *Nat Rev Dis Primer* 2019; **5**: 18.
27. Ostaszewski M, Niarakis A, Mazein A et al. COVID-19 Disease Map, a computational knowledge repository of virus-host interaction mechanisms. *Mol Syst Biol* 2021; **17**: e10851.
28. Akwii RG, Sajib MS, Zahra FT, Mikelis CM. Role of angiotensin-2 in vascular physiology and pathophysiology. *Cell* 2019; **8**: 471.
29. Perelson AS, Neumann AU, Markowitz M, Leonard JM, Ho DD. HIV-1 dynamics in vivo: Virion clearance rate, infected cell life-span, and viral generation time. *Science* 1996; **271**: 1582–1586.
30. Oczypok EA, Perkins TN, Oury TD. All the “RAGE” in lung disease: The receptor for advanced glycation endproducts (RAGE) is a major mediator of pulmonary inflammatory responses. *Paediatr Respir Rev* 2017; **23**: 40–49.
31. Cardeñoso Domingo L, Roy Vallejo E, Zurita Cruz ND et al. Relevant SARS-CoV-2 viraemia is associated with COVID-19 severity: Prospective cohort study and validation cohort. *J Med Virol* 2022; **94**: 5260–5270.
32. Jacobs JL, Naqvi A, Shah FA et al. Plasma SARS-CoV-2 RNA levels as a biomarker of lower respiratory tract SARS-CoV-2 infection in critically ill patients with COVID-19. *J Infect Dis* 2022; **226**: 2089–2094.
33. Li Y, Schneider AM, Mehta A et al. SARS-CoV-2 viraemia is associated with distinct proteomic pathways and predicts COVID-19 outcomes. *J Clin Invest* 2021; **131**: e148635.
34. Roy-Vallejo E, Cardeñoso L, Triguero-Martínez A et al. SARS-CoV-2 viraemia precedes an IL6 response in severe COVID-19 patients: Results of a longitudinal prospective cohort. *Front Med* 2022; **9**: 855639.
35. Andersson MI, Arancibia-Carcamo CV, Auckland K et al. SARS-CoV-2 RNA detected in blood products from patients with COVID-19 is not associated with infectious virus. *Wellcome Open Res* 2020; **5**: 181.
36. Tremblay K, Rousseau S, Zawati MH et al. The Biobanque québécoise de la COVID-19 (BQC19)—A cohort to prospectively study the clinical and biological determinants of COVID-19 clinical trajectories. *PLOS ONE*. 2021; **16**: e0245031.
37. Fong Y, Sebestyen K, Yu X, Gilbert P, Self S. nCal: An R package for non-linear calibration. *Bioinformatics* 2013; **29**: 2653–2654.
38. Mathworks. *Matlab 2022a*. Natick, Massachusetts: Mathworks; 2022.
39. Hill AL, Rosenbloom DIS, Nowak MA, Siliciano RF. Insight into treatment of HIV infection from viral dynamics models. *Immunol Rev* 2018; **285**: 9–25.
40. Keizer RJ, Jansen RS, Rosing H et al. Incorporation of concentration data below the limit of quantification in population pharmacokinetic analyses. *Pharmacol Res Perspect* 2015; **3**: e00131.
41. Savic RM, Mentré F, Lavielle M. Implementation and evaluation of the SAEM algorithm for longitudinal ordered categorical data with an illustration in pharmacokinetics–pharmacodynamics. *AAPS J* 2011; **13**: 44–53.
42. Chan PLS, Jacqmin P, Lavielle M, McFadyen L, Weatherley B. The use of the SAEM algorithm in MONOLIX software for estimation of population pharmacokinetic-pharmacodynamic-viral dynamics parameters of maraviroc in asymptomatic HIV subjects. *J Pharmacokinetic Pharmacodyn* 2011; **38**: 41–61.

Supporting Information

Additional supporting information may be found online in the Supporting Information section at the end of the article.



This is an open access article under the terms of the [Creative Commons Attribution-NonCommercial](https://creativecommons.org/licenses/by-nc/4.0/) License, which permits use, distribution and reproduction in any medium, provided the original work is properly cited and is not used for commercial purposes.